

Article

Modeling the Macrophage-Mediated Inflammation Involved in the Bone Fracture Healing Process

Imelda Trejo ^{*}, Hristo Kojouharov and Benito Chen-Charpentier 

Department of Mathematics, The University of Texas at Arlington, P.O. Box 19408, Arlington, TX 76019-0408, USA; hristo@uta.edu (H.K.); bmchen@uta.edu (B.C.-C.)

^{*} Correspondence: imelda.trejo@mavs.uta.edu; Tel.: +1-817-272-3261

Received: 14 November 2018; Accepted: 15 January 2019; Published: 17 January 2019



Abstract: A new mathematical model is presented to study the effects of macrophages on the bone fracture healing process. The model consists of a system of nonlinear ordinary differential equations that represents the interactions among classically and alternatively activated macrophages, mesenchymal stem cells, osteoblasts, and pro- and anti-inflammatory cytokines. A qualitative analysis of the model is performed to determine the equilibria and their corresponding stability properties. Numerical simulations are also presented to support the theoretical results, and to monitor the evolution of a broken bone for different types of fractures under various medical interventions. The model can be used to guide clinical experiments and to explore possible medical treatments that accelerate the bone fracture healing process, either by surgical interventions or drug administrations.

Keywords: bone repair; macrophages; immune system; cytokines; stem cells

1. Introduction

Bone fractures are becoming a serious worldwide problem, due to their high frequency and surgical complications. Globally, more than 8.9 million fractures occur every year, where 10–15% of them result in nonunion [1–5]. Prolonged healing, disabilities, and high morbidity rates are associated with severe traumas and immune-compromised-fractured people [2,3,6–8]. In addition, medical care costs for bone fractures are expected to be over US\$25 billions by 2025; due, in part, to the expensive treatments and prolonged hospitalization and rehabilitation [3,9]. It is essential to have a better understanding of the bone fracture healing process, in order to prevent unsuccessful healing and to develop optimal fracture union treatments.

Recently, experimental and mathematical models have demonstrated that macrophages strongly regulate bone fracture healing [10,11]. Depletion of macrophages results in delayed bone formation [12]. Furthermore, during inflammation, classically activated macrophages attract mesenchymal lineage cells (MSCs) to the injury site and activate the healing process [3,10,12]. In contrast, during the repair phase, alternatively activated macrophages promote MSC proliferation and differentiation, and accelerate bone healing [10,13]. However, the exact mechanisms by which macrophages contribute to bone healing remain unclear [3,10,14]. Also, the interaction between macrophages and tissue cells, as well as the importance of classically and alternatively activated macrophages during the bone healing process, are still not clearly understood [10,12,13].

In [11], a mathematical model, based on the interactions among macrophages, MSCs, and osteoblasts, was developed to study the regulatory effects of two generic pro- and anti-inflammatory cytokines during the early stages of bone fracture healing. To our knowledge, it was the first attempt to incorporate the macrophage interactions in the modeling of the bone fracture healing process. The mathematical model revealed that high concentrations of pro-inflammatory cytokines negatively affect the healing time of a fracture, while the administration of anti-inflammatory cytokines can accelerate the healing time in a

dose-dependent manner. Therefore, it is important to carefully consider and incorporate in the modeling approach all sources of pro- and anti-inflammatory cytokines, such as macrophages [2,3,15], in order to correctly represent the complex progression of the bone fracture healing process.

In this paper, the mathematical model developed in [11] is extended, to separately incorporate the two different phenotypes of macrophages: Classically and alternatively activated macrophages, as they have distinct functions during the healing process [10,15,16]. Classically activated macrophages release high levels of pro-inflammatory cytokines, including TNF- α and IL-1 β , which exhibit inhibitory and destructive properties in high concentrations [16,17]. In contrast, alternatively activated macrophages are characterized by the secretion of anti-inflammatory cytokines, such as IL-10, which increase their phagocytic activities, mitigate the inflammatory responses, promote growth, and accelerate fracture healing [2,3,15,16]. This extension leads to a more realistic model, by incorporating the different phagocytic rates and the separate production of the pro- and anti-inflammatory cytokines by the two types of macrophages [15,18]. The model can be used to investigate the macrophage functions during inflammation and their effects during the bone fracture healing process. The model can also be used to investigate potential therapeutic treatments, based on the use of anti-inflammatory cytokines, stem cells, and macrophages, suggesting possible ways to guide clinical experiments and bone tissue engineering strategies [15,16].

The organization of the paper is as follows: Section 2 discusses the cellular and molecular interactions that occur during the bone fracture healing process. The macrophage-mediated inflammation involved in the bone fracture healing process is also described in detail. The simplifying assumptions are presented in Section 3. In Section 4, a system of nonlinear ordinary differential equations is introduced, to mathematically describe the fundamental aspects of the bone fracture healing process during the resolution of inflammation and bone repair. The stability analysis of the system is presented in Section 5. Section 6 demonstrates the functionality of the model, by numerically simulating the progression of the bone fracture healing process under normal and pathological conditions. The discussion and future work are presented in Section 7.

2. Biological Background

Bone fracture healing is a complex biological process, which involves the participation of different cell types (including the immune system and mesenchymal lineage cells [16]) and is strongly regulated by released molecular factors [10,16,19–21]. Particularly, at the beginning of the healing process, cytokines activate and direct both immune and tissue cellular functions.

Cytokines are functionally classified into pro-inflammatory and anti-inflammatory families. Pro-inflammatory cytokines, such as the tumor necrotic factor- α (TNF- α), activate the immune system defense to kill bacteria and fight infections. Anti-inflammatory cytokines block the pro-inflammatory synthesis and activate the mesenchymal lineage cellular functions [2]. Interleukin-10 (IL-10) is one of the most potent anti-inflammatory molecules that inhibits pro-inflammatory production [2,22], and is mainly delivered by macrophages and MSCs [2]. A correct balance between pro- and anti-inflammatory cytokines during fracture healing is necessary for successful fracture repair. High levels of TNF- α induce chronic inflammation and gradual destruction of cartilage and bone tissue [21], while the absence of TNF- α results in nonunion or delayed nonunions [17,23].

Bone fracture healing can be described in three characteristic phases: Inflammatory, repair, and remodelling (see Figure 1) [24]. During inflammation, necroses of cells result in the delivery of pro-inflammatory cytokines which attract inflammatory immune cells, such as neutrophils and monocytes [1,23], to the injury site. In response to their phagocytic activities, these cells magnify the pro-inflammatory production, leading to an acute inflammation [17,23,25]. Subsequently, monocytes differentiate into macrophages to down-regulate the inflammation and resolve it. Once this differentiation begins, the influx of the inflammatory cells ceases, and they die out [26].

During the resolution of inflammation, macrophages increase their population by migration and activate to their classical and alternative phenotypes, accordingly to the cytokine stimuli [16,27].

The two phenotypes can also shift between each other during this process [28,29]. Macrophages have the capability to release both pro- and anti-inflammatory cytokines through their different phenotypes [28]. Classically activated macrophages release high concentration of pro-inflammatory cytokines, including $\text{TNF-}\alpha$, and low levels of anti-inflammatory cytokines [28], in response to their engulfing functions. Alternatively activated macrophages secrete high levels of IL-10 and low levels of $\text{TNF-}\alpha$, as they continue with the clearance of debris and the modulation of inflammation [28].

During the repair phase, migrating MSCs contribute with the delivery of IL-10, and proliferate or differentiate into fibroblasts, chondrocytes, and osteoblasts [2,30]. Fibroblasts and chondrocytes proliferate and release the fibrinous/cartilagenous extracellular matrix, which fills up the fracture gap [10,30,31] while osteoblasts proliferate and deposit the new bone, also called woven bone [30]. Bone deposit results from mineralized collagen and other proteins being delivered by the osteoblasts [10]. After bone mineralization, osteoblasts remain on the bone surface or differentiate into osteocytes, which become part of the bone extracellular matrix [32,33].

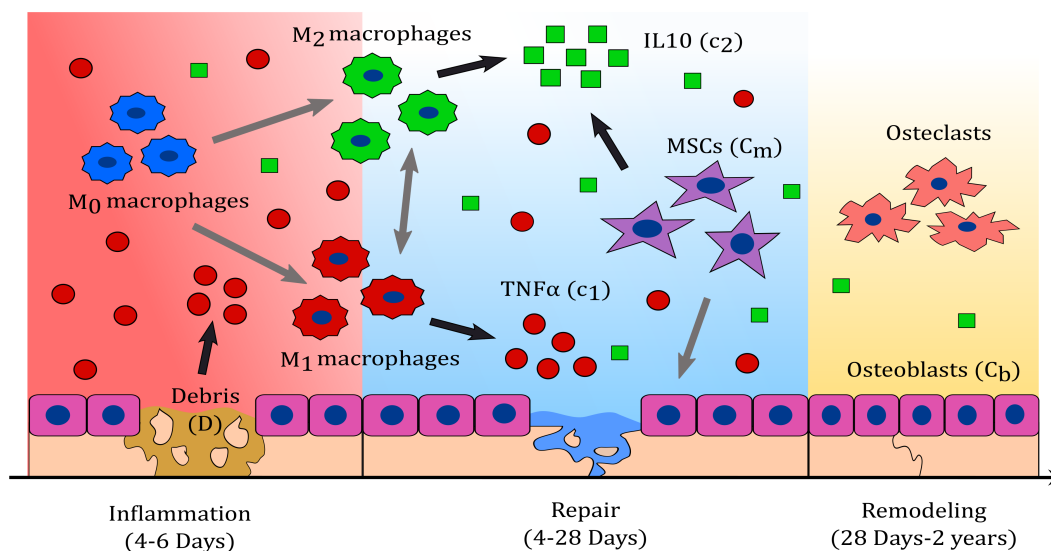


Figure 1. Inflammatory, repair, and remodeling phases of the bone fracture healing process. During the inflammatory phase, debris (D) activates the healing process by attracting macrophages M_0 to the injury site, which subsequently activate into their M_1 or M_2 phenotypes. Activated macrophages remove debris and secrete pro- and anti-inflammatory cytokines, such as tumor necrotic factor- α ($\text{TNF-}\alpha$) (c_1) and interleukin-10 (IL-10) (c_2), which regulate the inflammation and the cellular functions. During the repair phase, migrating mesenchymal stem cells (MSCs) up-regulate IL-10 production, proliferate, and differentiate into osteoblasts (C_b). Mesenchymal and osteoblast cells synthesize the fibro/cartilage and woven bone, which closes the fracture gap. During the bone remodeling phase, osteoblasts and osteoclasts constantly remove and deposit new bone until the fracture is fully repaired.

During the last phase of the bone fracture healing process, the fibrocartilage and the woven bone are constantly removed and replaced by a functional bone [34]. This process is referred to as bone remodeling, and consists of systematic tissue degradation and production by osteoclasts and osteoblasts, respectively. Bone remodeling is a slow process, that can take months to years until the bone recovers to its pre-injury state [14]. In a moderate fracture, acute inflammation is observed 24 h after the injury; it also corresponds to the peak of $\text{TNF-}\alpha$, which returns to baseline levels within 72 h [14,23]. Fibrinous/cartilagenous tissue production is observed in the first 3 days, peaks in about 10 to 12 days, and its removal starts as early as 21 days [30]. The inflammation is considered resolved when the debris is eliminated, activated macrophages emigrate to the lymphatic nodes to die, and inactivated macrophages return to their normal density [26]. These events are observed after two weeks from the beginning of the healing process [34,35]. At approximately 28 to 35 days, osteoclasts populate the injury site and a substantial removal of the fibrocartilage is observed [34]. The fracture healing

outcome is considered a delayed union if the fibrous/cartilaginous tissue is not removed completely in about 3 to 4 months after the injury, while it is considered a nonunion if no functional bone is obtained in 6 months after the trauma [36].

3. Modeling Assumptions

The most important effects of macrophages on bone fracture healing are observed during the inflammatory and repair phases of the healing process [11,16]. During the inflammatory phase, macrophages modulate and resolve the inflammation while, during the repair phase, macrophages provide an optimal environment for the cellular proliferation, differentiation, and tissue production. The primary variables during the inflammatory and repair phases of the bone fracture healing process are debris (D), unactivated macrophages (M_0), classical macrophages (M_1), alternative macrophages (M_2), MSCs (C_m), osteoblasts (C_b), pro-inflammatory cytokines (c_1), anti-inflammatory cytokines (c_2), fibrocartilage (m_c), and woven bone (m_b).

The biological system interactions are depicted in Figure 2. The cells and cellular dynamics are represented by the circular shapes and solid arrows. The molecular concentrations and their production/decay are represented by the octagonal shapes and dashed arrows. The pro- and anti-inflammatory cytokine activation/inhibition effects on the cellular functions are represented by the dotted arrows. Removal of debris and the negative effect among the variables are represented by the dot-ending dotted arrows.

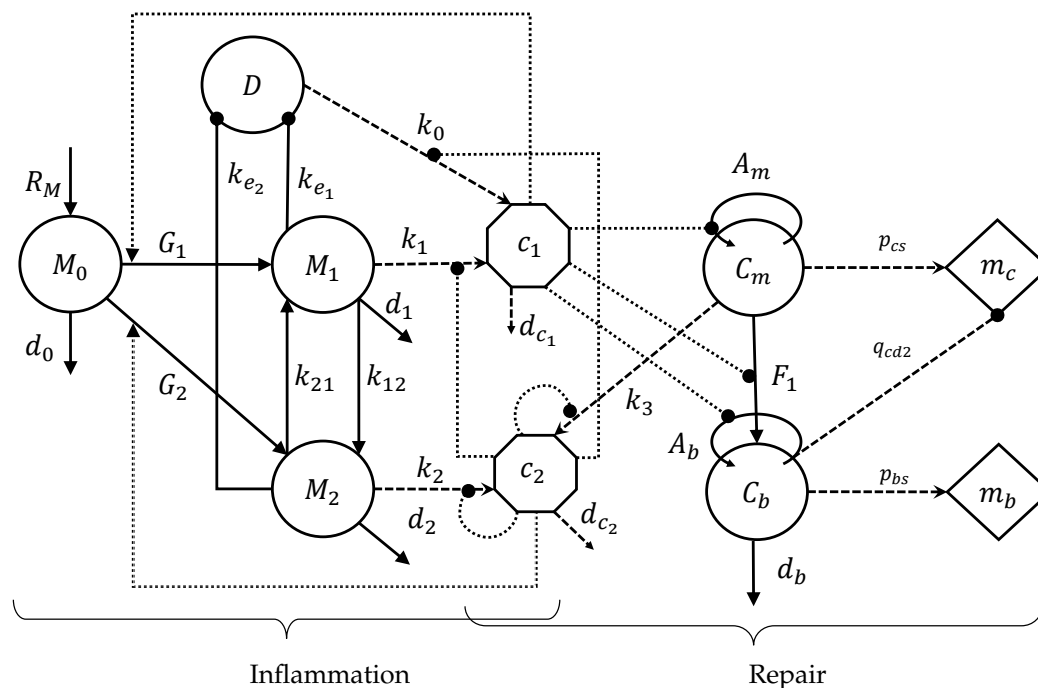


Figure 2. Flow diagram of the cellular and molecular dynamics during the inflammatory and repair phases of the bone fracture healing process.

It is assumed that the cellular functions are regulated by c_1 (such as $TNF-\alpha$) and c_2 (such as IL-10). It is also assumed that c_1 is delivered through cell necrosis and by the classically activated macrophages, while c_2 is delivered by the alternatively activated macrophages and MSCs. It is further assumed that the repair process is governed by the production of m_c and m_b [30,37], whose final levels are used to classify the outcome of the bone healing process. Additionally, it is assumed that the debris D are proportional to the number of necrotic cells [11]. It is also assumed that unactivated macrophages M_0 do not release cytokines and do not engulf debris. Additionally, the population of M_0 increases proportionally in size to the density of debris, up to a maximal value of M_{max} [27]. The only

source of activated macrophages, M_1 and M_2 , is M_0 . Even though both phenotypes of activated macrophages have the ability to release both pro- and anti-inflammatory cytokines, it is assumed that only M_1 deliver c_1 and M_2 deliver c_2 , as those are the major cytokines for each phenotype [38]. M_0 activate to M_1 under the c_1 stimulus, while they activate to M_2 under the c_2 stimulus. M_1 and M_2 macrophages do not de-differentiate back to the M_0 macrophages [39], and are able to switch phenotypes at a constant rate [29]. The accumulation of macrophages at the injury site is modeled by its recruitment due to inflammation, which is assumed to be proportional to the debris density.

Furthermore, it is assumed that the differentiation rates of MSCs into osteoblasts and osteoblasts into osteocytes are constant. MSCs synthesize the fibrocartilage, while osteoblasts synthesize the woven bone. It is also assumed that only the fibrocartilage is constantly removed by the osteoclasts, with the density of the osteoclasts being assumed proportional to the density of the osteoblasts [30]. In addition, it is assumed that the populations of the two tissue cells, C_m and C_b , experience logistic growth, where the growth rates decrease linearly as the population sizes approach a maximum value, K_{lm} and K_{lb} , respectively, imposed by the limited resources of the environment [30,40]. It is also assumed that there is no recruitment of MSCs and osteoblasts.

4. Model Formulation

The inflammatory and repair phases of the bone fracture healing process are modeled with a mass-action system of nonlinear ordinary differential equations. All variables represent homogeneous quantities in a given volume. Following the outlined biological assumptions and the flow diagram given in Figure 2 yields the resulting system of equations:

$$\frac{dD}{dt} = -R_D(k_{e1}M_1 + k_{e2}M_2) \tag{1}$$

$$\frac{dM_0}{dt} = R_M - G_1M_0 - G_2M_0 - d_0M_0 \tag{2}$$

$$\frac{dM_1}{dt} = G_1M_0 + k_{21}M_2 - k_{12}M_1 - d_1M_1 \tag{3}$$

$$\frac{dM_2}{dt} = G_2M_0 + k_{12}M_1 - k_{21}M_2 - d_2M_2 \tag{4}$$

$$\frac{dc_1}{dt} = H_1(k_0D + k_1M_1) - d_{c1}c_1 \tag{5}$$

$$\frac{dc_2}{dt} = H_2(k_2M_2 + k_3C_m) - d_{c2}c_2 \tag{6}$$

$$\frac{dC_m}{dt} = A_mC_m \left(1 - \frac{C_m}{K_{lm}}\right) - F_1C_m \tag{7}$$

$$\frac{dC_b}{dt} = A_bC_b \left(1 - \frac{C_b}{K_{lb}}\right) + F_1C_m - d_bC_b \tag{8}$$

$$\frac{dm_c}{dt} = (p_{cs} - q_{cd1}m_c)C_m - q_{cd2}m_cC_b \tag{9}$$

$$\frac{dm_b}{dt} = (p_{bs} - q_{bd}m_b)C_b \tag{10}$$

Equation (1) describes the rate of change with respect to time of the debris density, which decreases proportionally to M_1 and M_2 . The engulfing rate R_D is modeled by a Hill Type II function to represent the saturation of the phagocyte rate of macrophages [38,41]:

$$R_D = \frac{D}{a_{ed} + D}.$$

Equation (2) describes the rate of change with respect to time of the undifferentiated macrophages density. It increases because of migration and decreases by differentiating into M_1 and M_2 or by a

constant emigration rate. It is assumed that M_0 migrate to the injury site proportionally to D , up to a maximal constant rate, k_{max} , [22,28]:

$$R_M = k_{max} \left(1 - \frac{M}{M_{max}} \right) D,$$

where $M = M_0 + M_1 + M_2$. The differentiation rates of M_0 into M_1 and M_2 are stimulated by the cytokines accordingly to Hill Type II equations, respectively [29]:

$$G_1 = k_{01} \times \frac{c_1}{a_{01} + c_1}, \quad G_2 = k_{02} \times \frac{c_2}{a_{02} + c_2}.$$

Equation (3) describes the rate of change with respect to time of M_1 , which increases when M_0 activates to M_1 , and M_2 shifts phenotype; and decreases by emigration, and when M_1 shift phenotype. Similarly, Equation (4) describes the rate of change with respect to time of M_2 . Equations (5) and (6) describes the rate of change with respect to time of c_1 and c_2 . Here, k_0, k_1, k_2 , and k_3 are the constant rates of the cytokine productions and d_{c_1} and d_{c_2} are the cytokine constant decay rates. The inhibitory effects of the anti-inflammatory cytokines are modeled by the following functions [29]:

$$H_1 = \frac{a_{12}}{a_{12} + c_2}, \quad H_2 = \frac{a_{22}}{a_{22} + c_2}.$$

Equation (7) describes the rate of change with respect to time of C_m , which increases by cellular division up to a constant-maximal carrying capacity, K_{lm} , and decreases by differentiation [30]. The total MSC proliferation rate is modeled by [42]:

$$A_m = k_{pm} \times \frac{a_{pm}^2 + a_{pm}c_1}{a_{pm}^2 + c_1^2},$$

where in the absent of inflammation, $c_1 = 0$, MSC proliferate at a constant rate k_{pm} . However, when there is inflammation, $c_1 > 0$, and the proliferation rate of MSCs increases or decreases according to the concentration of c_1 (i.e., high concentration levels of c_1 inhibit C_m proliferation, while low concentration levels of c_1 accelerate C_m proliferation). The differentiation rate of C_m is inhibited by c_1 , which is modeled by the following function [11]:

$$F_1 = d_m \times \frac{a_{mb_1}}{a_{mb_1} + c_1}.$$

Equation (8) describes the rate of change with respect to time of C_b . It increases when MSC differentiate into osteoblasts, or when osteoblasts proliferate [30]. It decreases at a constant rate d_b when osteoblasts differentiate into osteocytes. The osteoblast proliferation rate is inhibited by c_1 , which is modeled by the following function [11]:

$$A_b = k_{pb} \times \frac{a_{pb}}{a_{pb} + c_1}.$$

Equations (9) and (10) describe the rate of change with respect to time of the fibrocartilage and woven bone, where p_{cs} and p_{bs} are the tissue constant synthesis rates and q_{cd1} , q_{cd2} , and q_{bd} are the tissue degradation rates, respectively [30].

5. Analysis of the Model

The analysis of Model (1)–(10) is done by finding the equilibria and their corresponding stability properties. An equilibrium is a state of the system where the variables do not change over time [40]. Once the equilibria are identified, it is important to determine the behavior of the model near the equilibria by analyzing their local stability properties. An equilibrium is locally stable if the system moves toward it when it is near the equilibrium, otherwise it is unstable [40]. Therefore, the equilibria provide the possible outcomes of the bone fracture healing process, and their corresponding stability properties define the conditions under which a particular healing result occurs.

System (1)–(10) has the following three biologically meaningful equilibria of the vector form $E = (D, M_0, M_1, M_2, c_1, c_2, C_m, C_b, m_c, m_b)$: $E_0 = (0, 0, 0, 0, 0, 0, 0, 0, m_{c_0}^*, m_{b_0}^*)$, $E_1 = (0, 0, 0, 0, 0, 0, 0, K_{Ib}(1 - d_b/k_{pb}), 0, p_{bs}/q_{bd})$, $E_2 = (0, 0, 0, 0, 0, c_2^*, C_m^*, C_b^*, m_c^*, p_{bs}/q_{bd})$, where $C_m^* = K_{Im}(1 - d_m/k_{pm})$, $C_b^* = K_{Ib}(k_{pb} - d_b + \sqrt{(k_{pb} - d_b)^2 + 4k_{pb}d_m C_m^*/K_{Ib}})/2k_{pb}$, $c_2^* = a_{22}(-1 + \sqrt{1 + 4k_3 C_m^*/a_{22}d_{c_2}})/2$, and $m_c^* = p_{cs} C_m^*/(q_{cd1} C_m^* + q_{cd2} C_b^*)$. The existence conditions for the three equilibria are summarized in Table 1 and their stability conditions are summarized in Table 2, and are proved in Appendix A.

The existence conditions, listed in Table 1, arise from the fact that all biologically meaningful variables are nonnegative. Therefore, the existence condition for E_0 requires the steady state tissue densities to be either zero or any positive number. For E_1 , the existence condition arises from the requirement that the steady state density of C_b must be greater than zero, which implies that the proliferation rate of osteoblasts must be greater than their differentiation rate (i.e., $k_{pb} > d_b$).

Similarly for E_2 , the existence condition arises from the requirement that the steady state density for C_m must be greater than zero, which implies that the proliferation rate of MSCs must be greater than their differentiation rate (i.e., $k_{pm} > d_m$).

Table 1. Existence conditions for the equilibrium points and their biological meaning.

Equilibrium Points	Existence Conditions	Meaning
$E_0 = (0, 0, 0, 0, 0, 0, 0, 0, m_{c_0}^*, m_{b_0}^*)$	$m_{c_0}^* \geq 0, m_{b_0}^* \geq 0$	nonunion
$E_1 = (0, 0, 0, 0, 0, 0, 0, K_{Ib}(1 - d_b/k_{pb}), 0, p_{bs}/q_{bd})$	$k_{pb} > d_b$	successful healing
$E_2 = (0, 0, 0, 0, 0, c_2^*, C_m^*, C_b^*, m_c^*, p_{bs}/q_{bd})$	$k_{pm} > d_m$	nonunion or delayed union

The stability conditions of each biologically feasible equilibrium are listed in Table 2, and is determined from the eigenvalues of its associated Jacobian matrix (see Appendix A), as follows:

E_0 is stable when $k_{pm} \leq d_m$ and $k_{pb} \leq d_b$ (see Theorem A1), which implies that the differentiation rates of the MSC and osteoblasts are greater than or equal to their proliferation rates, respectively. The steady-state E_0 represents a nonunion. In this case, the inflammation is resolved, since the first five entries of E_0 are zero; however, the repair process has failed since the osteoblasts and osteoclasts have died out before the beginning of the remodeling process. Hence, the tissue densities, $m_{c_0}^*$ and $m_{b_0}^*$, can be any two positive values smaller than their maximal densities, p_{cs}/q_{cd1} and p_{bs}/q_{bd} , respectively (see Theorem A1).

E_1 is stable when $k_{pm} \leq d_m$ and $k_{pb} > d_b$ (see Theorem A2). The steady-state E_1 represents a successful repair of the bone fracture, where the inflammation is resolved, the fibrocartilage is completely removed from the repair site, and the woven bone has achieved its maximal density. In this case, osteoblasts proliferate faster than they differentiate, while MSC have the opposite behavior.

E_2 is stable when $k_{pm} > d_m$ (see Theorem A3). The steady-state E_2 represents a nonunion or delayed union, where the inflammation is resolved, but the osteoclasts have failed to degrade the cartilage in a timely fashion.

Table 2. Stability conditions for the equilibrium points.

Equilibrium Points	Stability Conditions	Stability
E_0	$k_{pm} \leq d_m, k_{pb} \leq d_b$	E_0 belongs to an attracting local set
E_0, E_1	$k_{pm} \leq d_m, k_{pb} > d_b$	E_0 unstable; E_1 locally stable
E_0, E_2	$k_{pm} > d_m, k_{pb} \leq d_b$	E_0 unstable; E_2 locally stable
E_0, E_1, E_2	$k_{pm} > d_m, k_{pb} > d_b$	E_0 and E_1 unstable; E_2 locally stable

6. Numerical Results

The proposed new model (1)–(10) is used to study the importance of macrophages during the inflammatory and repair phases of the bone fracture healing process, which occur within the first 21 days after trauma [11,13]. It is also used to investigate the evolution of a broken bone under normal and pathological conditions. Table 3 summarizes the baseline parameter values and units for the numerical simulations. These values are estimated in a qualitative manner from data in other studies [11,27,30,38,39,43]. Some of those, from [11], were also rescaled to account for the different mathematical expressions of the proliferation and differentiation rates of the tissue cells. All parameter values are based on murine experiments, with healthy mice having a moderate fracture (a broken bone with a gap size less than 3 mm) [30,43]. However, the bone fracture healing process for humans involves the same cells, cytokines, and qualitative dynamics, differing only in the number of cells, concentrations, and the length of time it takes for a full recovery [24].

First, a set of numerical simulation results was presented to compare two mathematical models of the bone fracture healing process that incorporate macrophages: The model developed in [11], and the new model (1)–(10). Next, numerical simulations were performed to support the theoretical stability results (successful and nonunion equilibria) and to numerically monitor the healing progression of a moderate fracture in normal conditions. Another set of numerical simulations was performed to analyze the effects of different debris densities on bone fracture healing. Finally, a set of numerical simulation results was presented, to investigate the effects of different concentrations of anti-inflammatory cytokines and various cellular treatments on the fracture healing under numerous pathological conditions. All simulations were obtained by using the adaptive MATLAB solver `ode23s`, and were initiated with densities of debris, macrophages, and MSCs set to $D(0) = 5 \times 10^7$, $M_0(0) = 4000$, $C_m(0) = 1000$, respectively, and the pro-inflammatory cytokine concentration set to $c_1(0) = 1$.

6.1. Comparison of Existing Models

The model developed in [11] and the present mathematical model (1)–(10) were compared when $D(0) < a_{ed} = 4.71 \times 10^6$ (i.e., the initial debris concentration was below the half-saturation of debris). In this case, the macrophage digestion rate increased approximately linearly with respect to the debris population, as assumed in model [11]. The same parameter values were used in both models (Table 3), with $k_{e1} = 11$, $k_{e2} = 48$, $k_2 = 3.72 \times 10^{-6}$, $k_3 = 8 \times 10^{-6}$, and $q_{bd} = 5 \times 10^{-8}$.

Figure 3 shows the numerical evolutions of the tissues' production when $D(0) = 2 \times 10^6$. In all simulations, we refer to fibrocartilage and woven bone as cartilage and bone, respectively. The production of cartilage m_c and bone m_b given by the present model is much more realistic than the production given by the model developed [11], since, according to the experimental data, the cartilage production peaks to its maximal density of around 1 g/mL about 10–12 days after trauma, and significant bone tissue production is observed after the second week [44].

Table 3. Parameter descriptions and units.

Parameter	Description	Range of Values	Reference
k_{e1}	Engulfing debris rate of M_1	3–48/day	[38,41]
k_{e2}	Engulfing debris rate of M_2	3–48/day	[38,41]
a_{ed}	Half-saturation of debris	4.71×10^6 cells/mL	[38]
k_{max}	Maximal migration rate	0.015–0.1/day	[39,45]
M_{max}	Maximal macrophages density	6×10^5 – 1×10^6 cells/mL	[27,41]
k_{01}	Activation rate of M_1	0.55–0.611/day	[29,39]
k_{02}	Activation rate of M_0 to M_2	0.0843–0.3/day	[29]
k_{12}	Transition rate from M_1 to M_2	0.083–0.075/day	[29,39]
k_{21}	Transition rate from M_2 to M_1	0.005–0.05/day	[29]
d_0	Emigration rate of M_0	0.156–0.02/day	[29,39]
d_1	Emigration rate of M_1	0.121–0.2/day	[29,38,39]
d_2	Emigration rate of M_2	0.163–0.2/day	[29,38,39]
k_0	Secretion rate of c_1 by debris	5×10^{-7} – 8.5×10^{-6} ng/cells/day	[38]
k_1	Secretion rate of c_1 by M_1 macrophages	8.3×10^{-6} ng/cells/day	[38]
k_2	Secretion rate of c_2 by M_2 macrophages	3.72×10^{-6} ng/cells/day	[38]
k_3	Secretion rate of c_2 by MSCs	7×10^{-7} – 8×10^{-6} ng/cells/day	[11]
d_{c1}	Decay rate of c_1	12.79–55/day	[29,38]
d_{c2}	Decay rate of c_2	2.5–4.632/day	[29,38]
a_{12}	Effectiveness of c_2 inhibition of c_1 synthesis	0.025 ng/mL	[29]
a_{22}	Effectiveness of c_2 inhibition of c_2 synthesis	0.1 ng/mL	[29]
a_{pm}	Effectiveness of c_1 inhibition of C_m proliferation	3.162 ng/mL	[11,46]
a_{mb1}	Effectiveness of c_1 inhibition of C_m differentiation	0.1 ng/mL	[11,47]
a_{01}	Half-saturation of c_1 to activate M_1	0.01 ng/mL	[29]
a_{02}	Half-saturation of c_2 to activate M_2	0.005 ng/mL	[29]
a_{pb}	Effectiveness of c_1 inhibition of C_b proliferation	10 ng/mL	[11,48]
a_{pm1}	Constant enhancement of c_1 to C_m proliferation	13 ng/mL	[11,46]
k_{pm}	Proliferation rate of C_m	0.5/day	[11]
d_m	Differentiation rate of C_m	1/day	[11,30]
k_{pb}	Proliferation rate of C_b	0.2202/day	[11,30]
d_b	Differentiation rate of C_b	0.15/day	[11,30]
p_{cs}	Fibrocartilage synthesis rate	3×10^{-6} g/cells/day	[11,30]
q_{cd1}	Fibrocartilage degradation rate	3×10^{-6} mL/cells/day	[11,30]
q_{cd2}	Fibrocartilage degradation rate by osteoclasts	0.2×10^{-6} mL/cells/day	[11,30]
p_{bs}	Bone tissue synthesis rate	5×10^{-8} g/cells/day	[11,30]
q_{bd}	Bone tissue degradation rate	5×10^{-8} mL/cells/day	[30]
K_{Ib}	Carrying capacity of C_b	1×10^6 cells/mL	[11,30]
K_{Im}	Carrying capacity of C_m	1×10^6 cells/mL	[11,30]
$D(0)$	Density of necrotic cells	1×10^6 – 2×10^8 cells/mL	[27,38,41]
$C_m(0)$	Initial MSCs density	1000 cells/mL	[11]
$M_0(0)$	Unactivated macrophage density	4000 cell/mL	[45]

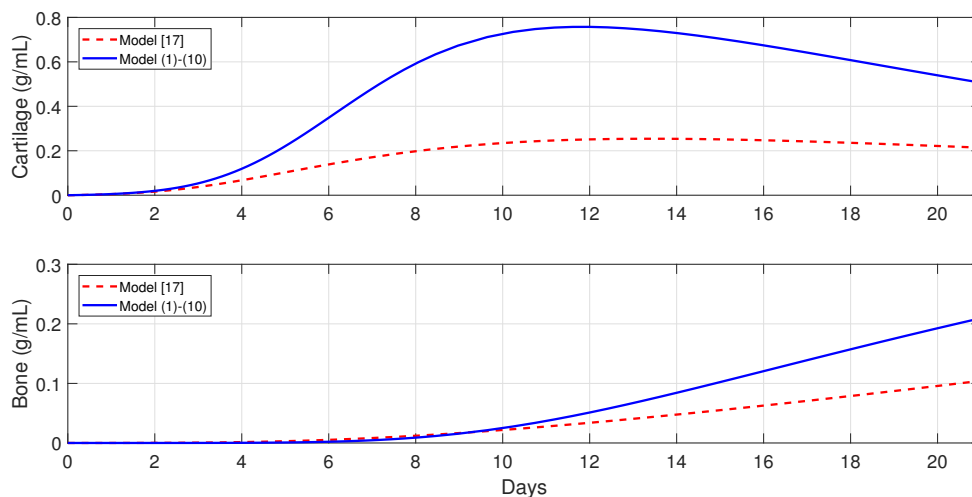


Figure 3. Comparison of tissues evolution in Model [11] and Model (1)–(10).

6.2. Different Outcomes of the Bone Fracture Healing Process

Next, a set of numerical simulations is presented to support the theoretical results. Accordingly to the qualitative analysis of the model there are three equilibria: E_0 , E_1 , and E_2 , where their stability conditions are determined by the tissue cells' proliferation and differentiation rates, k_{pm} , k_{pb} , d_m and d_b , respectively. The following parameter values were used: $k_{pm} = 0.5$, $d_m = 1$, $k_{pb} = 0.2202$, and $d_b = 0.3$, to demonstrate the stability of E_0 , since then $k_{pm} < d_m$ and $k_{pb} < d_b$. The stability of E_1 was demonstrated using the following parameter values: $d_m = 1$, $k_{pm} = 0.5$, $k_{pb} = 0.2202$, and $d_b = 0.15$, since then $k_{pm} \leq d_m$ and $k_{pb} > d_b$. Finally, the following parameter values were used: $k_{pm} = 0.5$ and $d_m = 0.1$, to demonstrate the stability of E_2 , since then $k_{pm} > d_m$. Different time-periods are used in Figures 4–6 to better demonstrate the qualitative behavior of the system under different stability conditions.

Figure 4 shows the qualitative behavior of E_1 for the macrophages, debris, TNF- α , and IL-10 densities, with the inflammation being resolved in about 40 days. The top-left plot of Figure 4 shows the temporal evolution of M_0 (dashed lines), M_1 (dotted lines), and M_2 (solid lines). It can be observed that M_1 first peaks to its maximum value, which is then followed by M_2 . Similar sequences of transitions of first M_1 , and then M_2 , are commonly observed in normal tissue healing conditions [2,39].

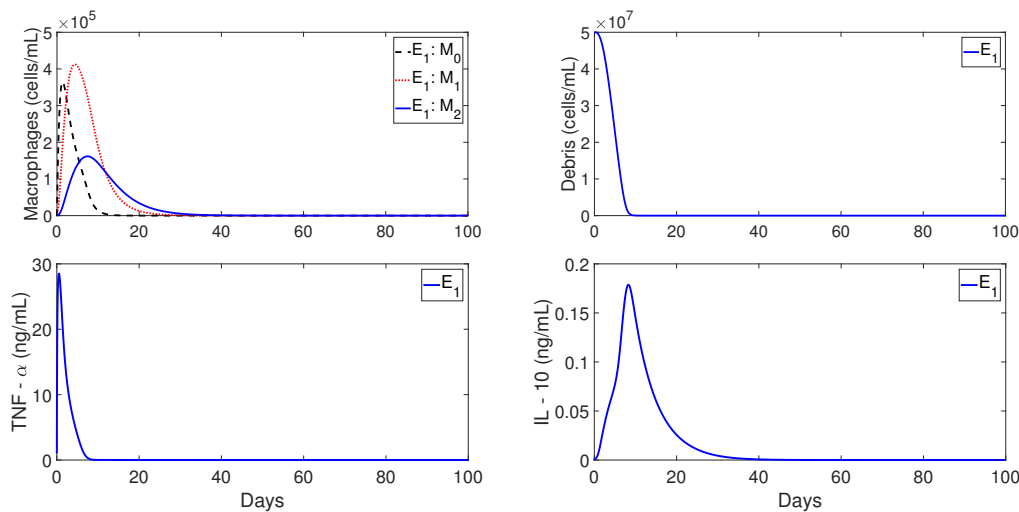


Figure 4. Cellular and molecular evolution of the resolution of the inflammation in normal conditions.

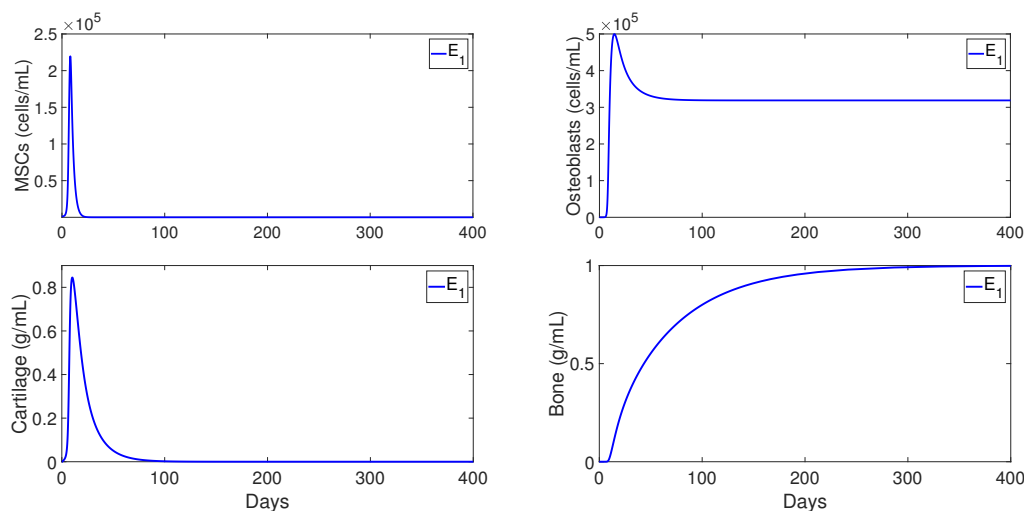


Figure 5. Cellular and molecular evolution of the repair process in a successful fracture healing.

Figure 5 shows the qualitative behaviors of E_1 for the MSC, osteoblasts, cartilage, and bone densities. Here, the MSC density decayed to zero over time, while the osteoblasts maintained a constant density below their carrying capacity $K_{lb} = 1 \times 10^6$. In addition, the bottom plots of Figure 5 shows that the cartilage was eventually degraded by the osteoclasts and the bone achieved its maximum density of 1 ng/mL. Therefore, E_1 exhibits the temporal progression of a successful bone fracture healing.

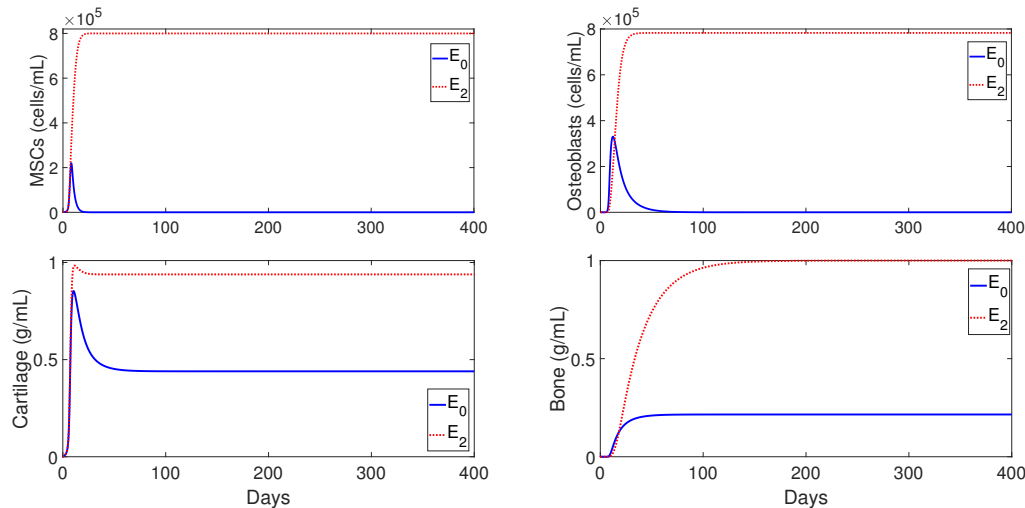


Figure 6. Cellular and molecular evolution of the repair process in a nonunion fracture healing.

Figure 6 shows the qualitative evolution for the MSC, osteoblasts, cartilage, and bone densities for E_0 (solid lines) and E_2 (dotted lines). Since the temporal evolution of macrophages, debris, and cytokines densities in E_0 and E_2 are similar to those for E_1 showed in Figure 4, they are omitted here. It can be observed, in Figure 6, that the two cellular densities in E_0 , MSC, and osteoblasts, decayed to zero over time, with the osteoclasts failing to degrade the cartilage; this results in nonunion. Mathematically, this case occurs when osteoblasts proliferate at a rate lower than their differentiation rate, i.e., $k_{pb} < d_b$. In practice, this scenario is commonly observed in advanced-age patients whose MSC and osteoblast cells decrease their capability to proliferate and differentiate [3]. On the other hand, the two cells and the two tissues in E_2 remain at positive constant values (Figure 6), but the final fracture healing outcome is still a nonunion. Here, the osteoclasts again fail to degrade the cartilage [3], even though the bone has achieved its maximum density of 1 ng/mL. Therefore, in this case, migration of osteoclasts must be enhanced through surgical interventions, in order to achieve a successful bone repair [30].

6.3. Importance of Macrophages during the Bone Fracture Healing Process

In this section, the mathematical model is used to investigate the effects of macrophages during the inflammatory and repair phases of the bone fracture healing process. The major contribution of macrophages to fracture healing is through the delivery of pro- and anti-inflammatory cytokines at the repair site. Therefore, the values of the parameters k_i , representing the secretion rates of c_i by M_i , $i = 1, 2$, are varied in the numerical simulations, as compared to their base values from Table 3.

Figure 7 shows that macrophages have a drastic effect on the short-term tissue dynamics during the healing process. In the presence of M_1 and M_2 , fibrocartilage formation more than doubles in about 1 week, while woven bone experiences an additional steady increase during the same period and beyond. The simulations presented in Figure 8 demonstrate the individual effects of the different phenotypes of macrophages, and show that the alternatively activated macrophages M_2 have a more dominant contribution to the tissue production, as compared to the classically activated macrophages M_1 .

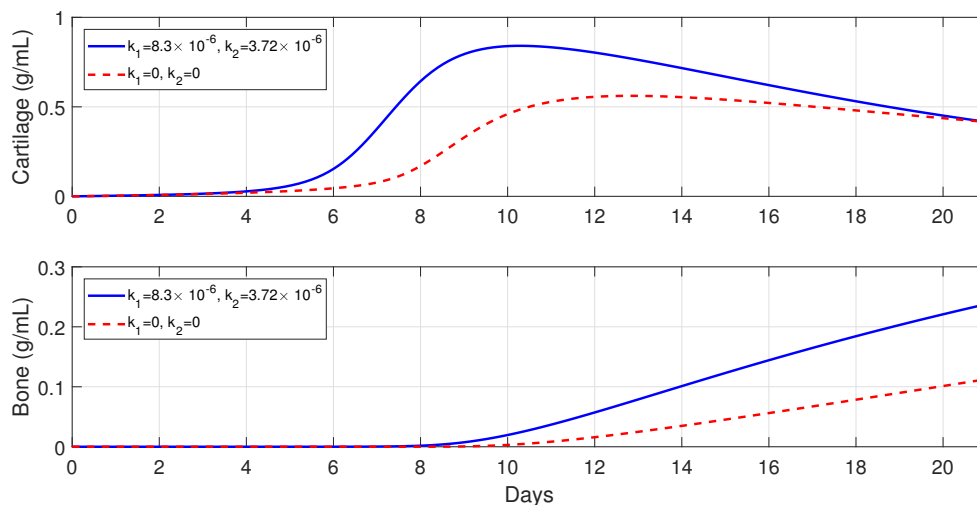


Figure 7. Tissue evolution when macrophages contribute to the healing process (solid line), $k_1, k_2 \neq 0$, and when they do not contribute to the healing process (dashed line), $k_1 = k_2 = 0$.

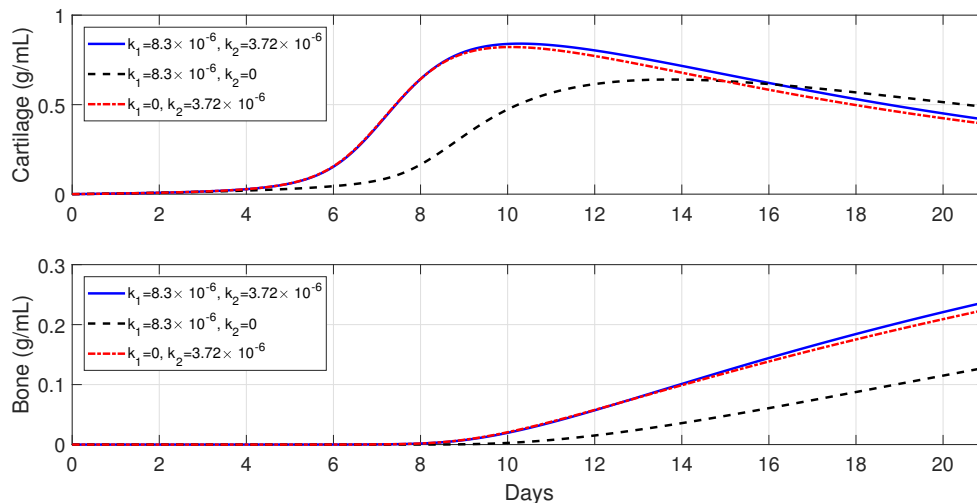


Figure 8. Tissue evolution when the alternatively activated macrophages, M_2 , do not contribute to the healing process (dashed line), $k_2 = 0$, and when the classically activated macrophages, M_1 , do not contribute to the healing process (dotted line), $k_1 = 0$.

6.4. Evolution of the Healing Process for Different Types of Fractures

In this section, the model is used to monitor the evolution of a successful repair (Table 3) for different types of fractures. In healthy individuals, simple, moderate, and severe fractures are correlated with the debris densities [49,50]. Therefore, the initial debris concentration is set to $D(0) = 3 \times 10^5$, $D(0) = 5 \times 10^7$, and $D(0) = 2 \times 10^8$, for a simple, moderate, and severe fracture, respectively.

Figure 9 shows that the tissue production is a slow process for a simple fracture, since the cartilage and bone densities are less than the corresponding tissue densities for moderate and severe fractures. A slow healing process is commonly observed in micro-crack healing [49]. Furthermore, there is less cartilage formation over time in simple fractures [50]. For a moderate fracture, the maximal production of cartilage is observed around 10 days, followed by a significant degradation, while the bone tissue production occurs after the first week. For a severe fracture, Figure 9 shows that there is a delay in the two tissues' production, compared with those given by moderate fractures, with the peak of the cartilage and bone production observed at around day 16.

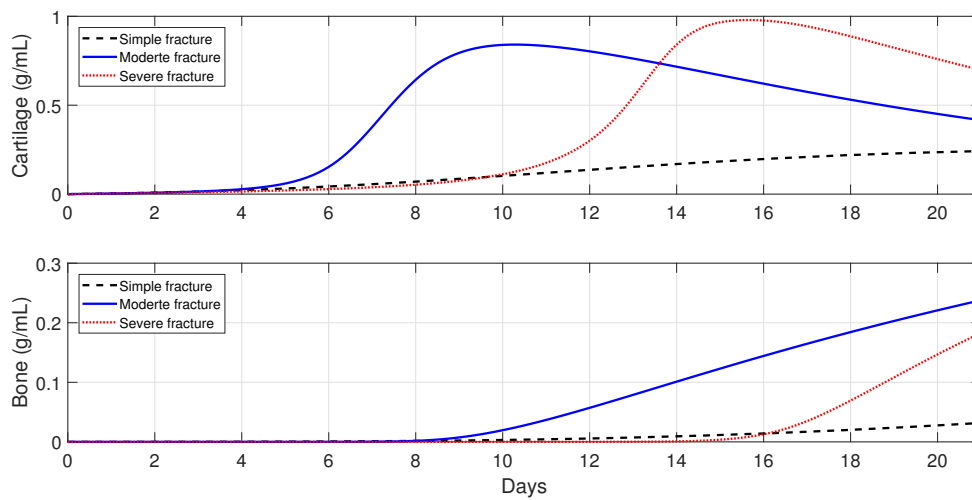


Figure 9. Tissue evolution of a successful repair for different types of fractures.

6.5. Immune-Modulation Therapeutic Treatments of Bone Fractures

The administration of anti-inflammatory drugs and the injection and/or transplantation of MSC and macrophages are two of the clinical trials that have been implemented in orthopedics to stimulate and accelerate bone fracture healing [2,23]. In this section, Model (1)–(10) is used to explore these possible therapeutic treatments to accelerate the healing of a broken bone, under normal and pathological conditions such as severe fractures, advanced age, and senile osteoporosis [3].

6.5.1. Administration of Anti-Inflammatory Drugs at the Beginning of the Healing Process

Treatments based on anti-inflammatory cytokines, such as the cytokine-specific agents that block the pro-inflammatory cytokines productions, have exhibited promising clinical results and have led to intense orthopedic research activities [1,2,17,23,33,51–53]. In this section, a set of numerical simulations is presented to investigate the effect of the administrations of anti-inflammatory cytokines at the beginning of the healing process in healthy individuals and also in immune-compromised patients. In each case of the numerical simulations, $c_2(0) = 0, 10,$ and 100 ng/mL .

In healthy individuals, the administration of anti-inflammatory drugs is implemented for a simple fracture and also for two moderate fractures with different debris concentrations: $D(0) = 3 \times 10^5,$ $D(0) = 2 \times 10^7,$ and $D(0) = 5 \times 10^7$.

Figure 10 shows that the administration of c_2 in the simple fracture slows down both the cartilage and bone productions. Figures 11 and 12 show that the administration of c_2 in the moderate fractures improves the tissue evolution, but in a dose-dependent manner. On one hand, when $D(0) = 2 \times 10^7,$ the administration of c_2 has either a positive or negative effect on the two tissue productions. The administration of 10 ng/mL of c_2 enhances the early production of cartilage and increases the bone synthesis, while the administration of 100 ng/mL of c_2 results in the opposite effect. On the other hand, when $D(0) = 5 \times 10^7,$ the administration of c_2 enhances the earlier cartilage production and improves the synthesis of the bone for both concentrations, with 10 ng/mL being the optimal of the two doses.

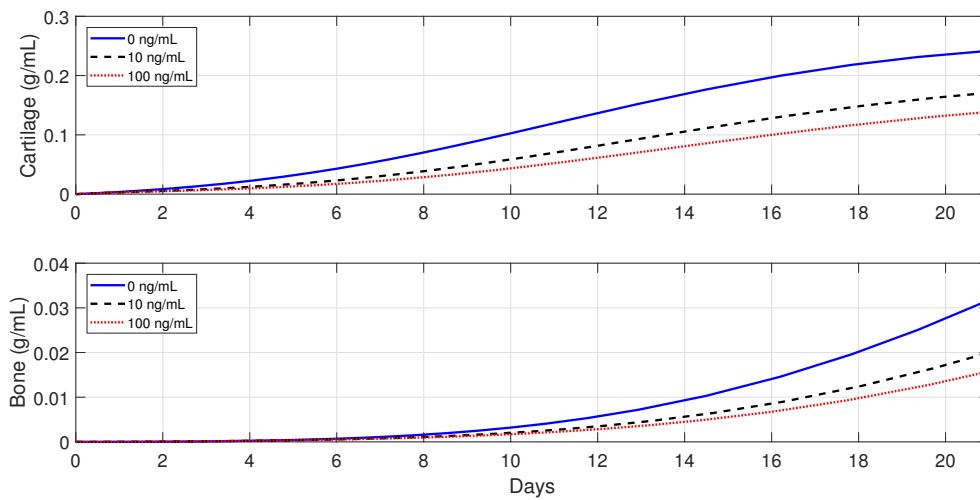


Figure 10. Tissue evolution in a simple fracture under different initial anti-inflammatory cytokines concentrations, $D(0) = 3 \times 10^5$.

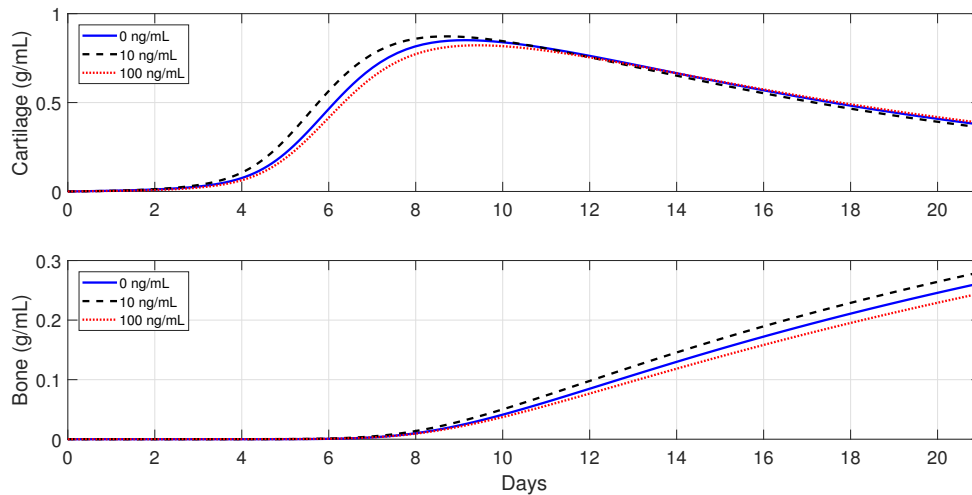


Figure 11. Tissue evolution in a moderate fracture under different initial anti-inflammatory cytokines concentrations, $D(0) = 2 \times 10^7$.

Next, the model is used to implement the administration of anti-inflammatory drugs under different pathological conditions. First, severe fractures in immune-compromised individuals are simulated by using the following parameter values: $D(0) = 2 \times 10^8$ and $k_{max} = 0.0015$, since, in the fractures of such individuals, there is an increase in the accumulation of debris [50] and a decrease in the macrophage migration rate [54]. Second, the following parameter values are used: $k_{e1} = k_{e2} = 3$ and $k_1 = 9 \times 10^{-6}$, to simulate bone fracture healing in aging individuals, since, in this case, the macrophage phagocytic rate decreases and there is an increase of pro-inflammatory cytokine synthesis by M_1 [3,25]. Finally, $c_1(0) = 100$, $k_{pm} = 0.2$, $d_m = 0.5$, $k_{pb} = 0.16$, and $d_b = 0.15$ are used to simulate the healing process for an senil osteoporotic fracture, since, in this case, a high level of pro-inflammatory cytokines is observed and the MSC and osteoblast functions decrease [3].

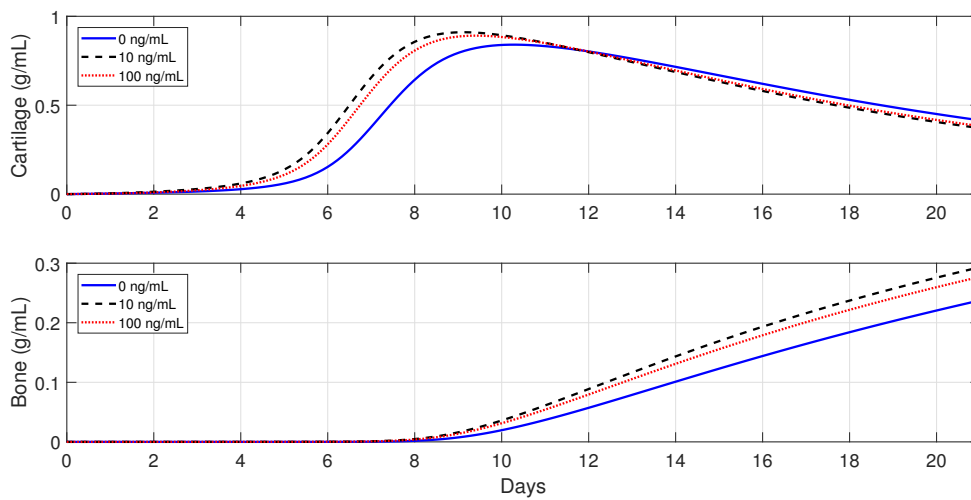


Figure 12. Tissue evolution in a moderate fracture under different initial anti-inflammatory cytokine concentrations, $D(0) = 5 \times 10^7$.

Figures 13–15 show that the administration of anti-inflammatory cytokines under the above three different pathological conditions always improve tissue productions, where the optimal dose of c_2 , for both the advanced-age individuals and senile osteoporotic fractures, is 10 ng/mL.

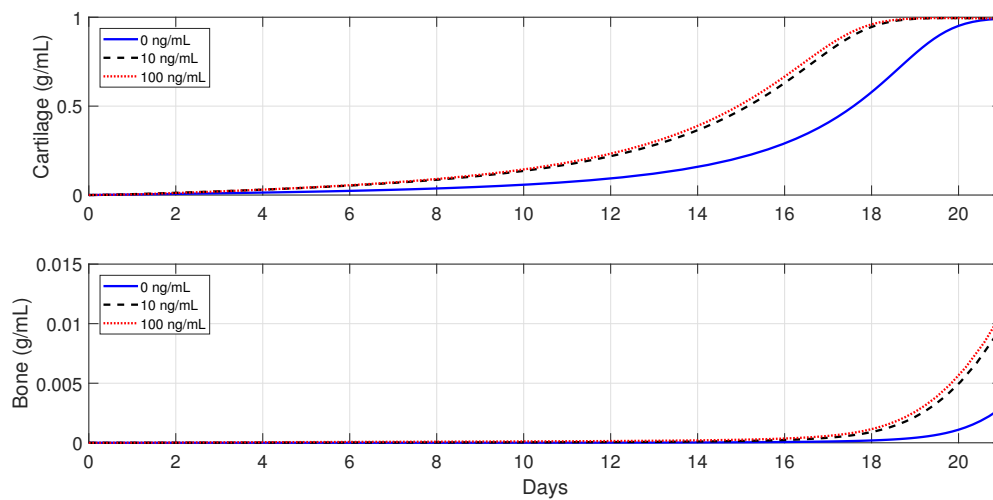


Figure 13. Tissue evolution in a severe fracture under different initial anti-inflammatory cytokines concentrations.

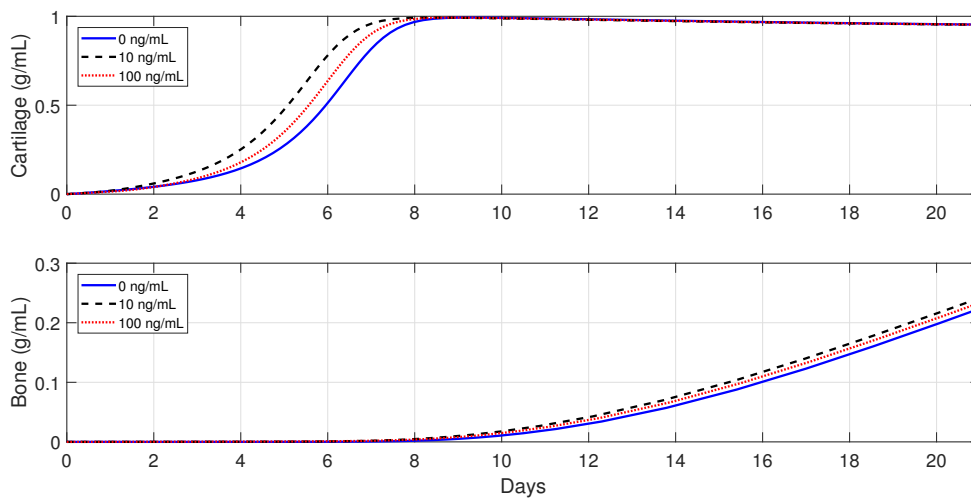


Figure 14. Tissue evolution in an advanced age fracture under different initial anti-inflammatory cytokines concentrations.

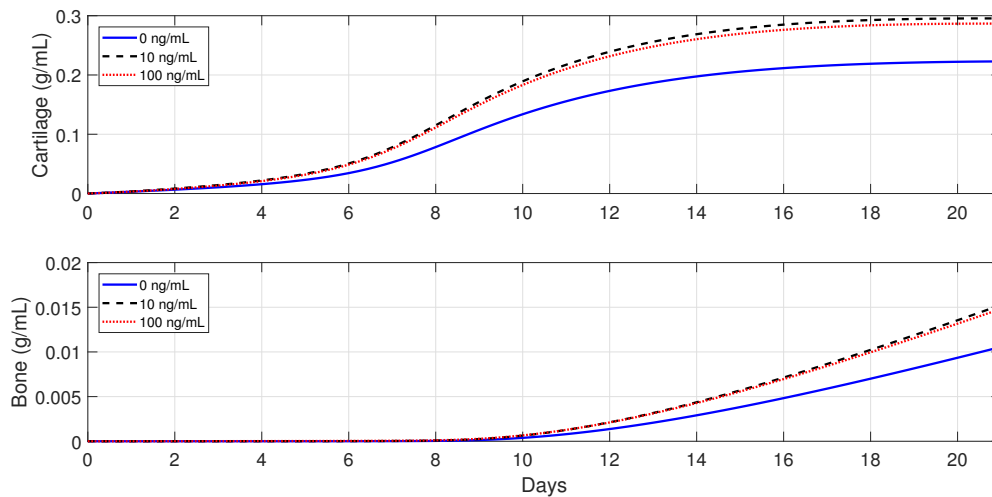


Figure 15. Tissue evolution in a senile osteoporotic fracture under different initial anti-inflammatory cytokines concentrations.

6.5.2. Cellular Therapeutic Interventions under Immune-Compromised Conditions

Additions of MSC to the injury site through injection and/or transplantation have been used in practice to stimulate and augment bone fracture healing [2]. Another cellular intervention is scaffold implants, where undifferentiated macrophages and MSCs are co-cultured together, and cytokines are slowly released to stimulate M_2 activation [3]. The parameter values used in the numerical simulations that explore these possible therapeutic treatments are the same as in Section 6.5.1.

For severe fractures with immune-compromised conditions, the use of scaffold implants is simulated through a fast M_2 activation (i.e., $k_{02} = 0.3$ and $k_{12} = 0.075$), and also an increase in the C_m and M_0 densities (i.e., $M_0(0) = 5000$ and $C_m(0) = 5000$). For fractures in aging individuals and individuals with senile osteoporotic fractures, the MSC injection and the fast M_2 activation are simulated by setting $C_m(0) = 5000$, $k_{02} = 0.3$, and $k_{12} = 0.075$.

Figures 16–18 show that the two cellular interventions increase both tissue productions. Furthermore, those interventions result in larger improvements in severe and senile osteoporotic fractures, when compared to fractures in aging individuals.

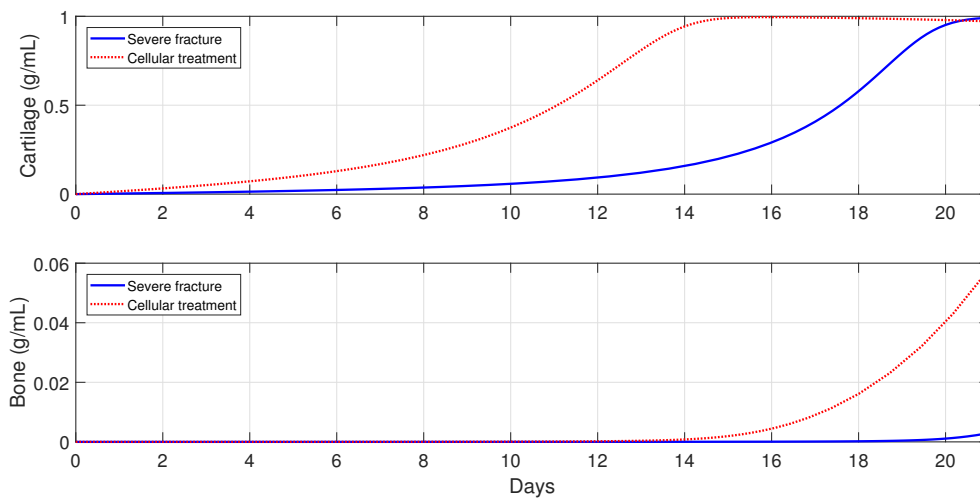


Figure 16. Tissue evolution in a severe fracture without therapeutic innervation (solid line) and with $M_0(0)$ and $C_m(0)$ transplantation (dotted line).

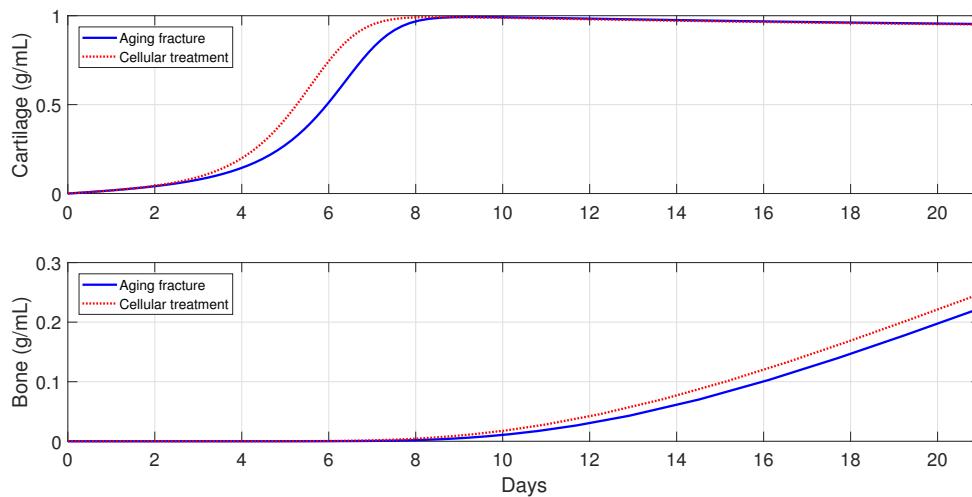


Figure 17. Tissue evolution in an aging fracture without therapeutic innervation (solid line) and with MSCs injection (dotted line).

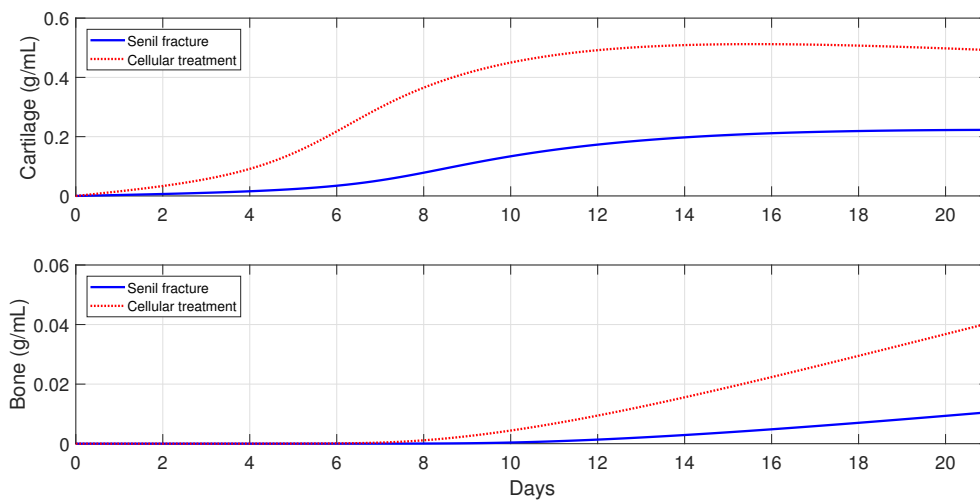


Figure 18. Tissue evolution in a senile osteoporotic fracture without therapeutic innervation (solid line) and with MSCs injection (dotted line).

7. Discussion and Conclusions

A new mathematical model was introduced to mathematically and numerically study the macrophage-mediated inflammation involved in the early stages of the bone fracture healing process: The inflammatory and repair phases. Classically and alternatively activated macrophages were incorporated in the model, to study their capabilities to modulate and resolve the inflammation. The model also included the macrophage abilities to regulate the tissue cellular functions through the delivery of pro- and anti-inflammatory cytokines. The resolution of the inflammation was assumed to be initiated with the activation of the macrophages into their classical phenotype. The classically activated macrophages deliver pro-inflammatory cytokines, such as $\text{TNF-}\alpha$, as they engulf debris. Then, the alternatively activated macrophages and the MSC modulate the inflammation by releasing anti-inflammatory cytokines, such as IL-10. Finally, the classically activated macrophages remove the remaining debris. The model also incorporated different engulfing rates of activated macrophages, saturation rates of phagocytes, and the maximal density of macrophages at the injury site, thus allowing a better understanding of the interplay between macrophages and tissue cells during the bone fracture healing process.

The mathematical analysis revealed that there are three feasible fracture healing outcomes. Two of the outcomes represent a nonunion healing: One is the case when the cells deactivate or die out before the healing process finishes up, and the other is the case when the tissue cells remain constant but the osteoclasts fail to completely remove the cartilage. The third outcome represents a successful healing, where the osteoblasts and osteoclasts are constantly producing and removing the woven bone. The stability conditions of each outcome can be used to biologically explain why the fracture healing fails, as well as to design therapeutic interventions to stimulate or accelerate the healing process.

The new model was used to study the importance of macrophages during the early stages of tissue production. It revealed that macrophages significantly improve the tissue production, with alternatively activated macrophages having the main effect on the process. The flexibility of the model also allowed us to perform a variety of different types of numerical simulations quickly and cost effectively. It was used to monitor the progression of the healing of a broken bone and to predict its final outcome. In particular, the administration of anti-inflammatory drugs to improve the bone fracture healing process was numerically simulated. It was found that the administration of anti-inflammatory cytokines fails to accelerate the healing process in simple fractures, while it accelerates the healing process in moderate fractures, depending on the cytokine concentrations, and always improves the healing process in severe fractures. Such results have been also clinically observed, when corticosteroids and nonsteroidal anti-inflammatory drugs (NSAIDs) are administered in bone fractures [23]. Therefore, based on the model findings, the concentration of debris must be carefully considered when administering anti-inflammatory drugs to enhance the fracture healing process [50]. The model was also used to explore other potential cellular therapeutic approaches, such as MSC injection and transplantation. It was found that such treatments can also improve the healing time of a broken bone, especially in immune-compromised patients. The model can also be easily adapted to other therapeutic approaches, such as the administration of different anti-inflammatory drugs, suggesting a variety of possible ways to guide clinical experiments and bone tissue engineering strategies.

Future research directions include modifications of the model by incorporating additional molecular and cellular interactions and processes during the inflammatory and repair phases of fracture healing, such as macrophage migration and MSC differentiation due to cytokine stimulus. Another research direction is the incorporation of the bone remodeling phase of the healing process, which begins at the end of the repair phase and continues long after fracture union. There are different factors that affect the bone remodeling, including other bone cells, such as osteoclasts, osteocytes, progenitor cells, and other sources of cytokines [30,32,43]. This presents a challenging new research direction in the pursuit to better understand the bone fracture healing process and the development of new treatment strategies.

Author Contributions: All authors contributed equally to the work reported.

Funding: This research was funded by Consejo Nacional de Ciencia y Tecnología grant No. Beca 383167.

Acknowledgments: The first author, I.T., was supported by the Mexico’s CONACyT and the University of Texas at Arlington.

Conflicts of Interest: The authors declare no conflict of interest. The founding sponsors had no role in the design of the study; in the collection, analyses, or interpretation of data; in the writing of the manuscript, and in the decision to publish the results.

Appendix A

The stability conditions of the equilibria of Model (1)–(10) are stated and proved below. The analysis is conducted using the Jacobian of the system at each equilibrium point and finding its corresponding eigenvalues [40,55].

Theorem A1. *The $E_0 = \{(0, 0, 0, 0, 0, 0, 0, 0, m_{c_0}^*, m_{b_0}^*)\}$ belongs to the set $B = \{(0, 0, 0, 0, 0, 0, 0, 0, m_c, m_b) : 0 \leq m_c \leq p_{cs}/q_{cd_1}, 0 \leq m_b \leq p_{bs}/q_{bd}\}$, which is a local attractor set of the solution set given by System (1)–(10) if and only if $k_{pm} \leq d_m$ and $k_{pb} \leq d_b$.*

Proof of Theorem A1. The right-hand side functions of System (1)–(10) are continuous and bounded, since all model variables and parameters are positive. Hence, for each initial condition of the system, there is a unique solution [55]. Then, as zero is a solution of the System (1)–(10), and by uniqueness of solution, all the solutions of the system with positive initial condition are positive [55].

Next, it will be proved that the hyperplane $A = \{(0, 0, 0, 0, 0, 0, 0, 0, m_c, m_b) : m_c \geq 0, m_b \geq 0\}$ is an attractor set of the solutions of the system (1)–(10). There are two cases to consider, based on the relation between the cell proliferation and differentiation rates.

First, let us examine the case when $k_{pm} < d_m$ and $k_{pb} < d_b$. The Jacobian matrix $J(E_0)$ is given by the following lower triangular block matrix

$$J(E_0) = \begin{pmatrix} J_1(E_0) & \mathbf{0} & \mathbf{0} \\ * & J_2(E_0) & \mathbf{0} \\ \mathbf{0} & * & J_3(E_0) \end{pmatrix},$$

where

$$J_1(E_0) = \begin{pmatrix} 0 & 0 & 0 & 0 \\ k_{max} & -d_0 & 0 & 0 \\ 0 & 0 & J_{11} & 0 \\ k_0 & 0 & * & -d_{c_1} \end{pmatrix}, \quad J_2(E_0) = \begin{pmatrix} -d_{c_2} & k_3 & 0 \\ 0 & -d_m + k_{pm} & 0 \\ 0 & d_m & -d_b + k_{pb} \end{pmatrix}$$

$$J_{11} = \begin{pmatrix} -d_1 - k_{12} & k_{21} \\ k_{12} & -d_2 - k_{21} \end{pmatrix}, \quad J_3(E_0) = \begin{pmatrix} 0 & 0 \\ 0 & 0 \end{pmatrix}.$$

Therefore, the corresponding characteristic polynomial associated with $J(E_1)$ is given by the product of the characteristic polynomials associated with each submatrix [56]:

$$p(\lambda) = \lambda^3 (\lambda + d_0) (\lambda + d_{c_1}) (\lambda + d_{c_2}) (\lambda + d_m - k_{pm}) (\lambda + d_b - k_{pb}) (\lambda^2 + a\lambda + b),$$

where $a = d_1 + d_2 + k_{12} + k_{21}$ and $b = k_{12}d_2 + k_{21}d_1 + d_1d_2$. The polynomial factor of order two of $p(\lambda)$ has the following two roots: $(-a \pm \sqrt{a^2 - 4b})/2$, which are negative since $a^2 - 4b = (d_1 - d_2 + k_{12} - k_{21})^2 + 4k_{12}k_{21} > 0$ and $b > 0$. Therefore, the eigenvalues of $J(E_0)$ are negative for the variables $M_0, M_1, M_2, c_1, c_2, C_m,$ and C_b and are equal to zero for $D, m_c,$ and m_b . Since $D'(t) \leq 0$ for all the variables in the system (1)–(10) and $(D^*, 0, 0, 0, 0, 0, 0, 0, m_c, m_b)$ with $D^* \neq 0$ is not an equilibrium point, then the solutions of the system (1)–(8) are attracted to the set $A = \{(0, 0, 0, 0, 0, 0, 0, 0, m_c, m_b) : m_c \geq 0, m_b \geq 0\}$.

Equations (9) and (10) imply that $m'_c \leq 0$ and $m'_b \leq 0$ for all $m_c > p_{cs}/q_{cd1}$ and $m_b > p_{bs}/q_{bd}$. Therefore, the set B is a local attractor set of A [55].

Next, let us consider the case when $k_{pm} = d_m$ and $d_b = k_{pb}$. Here, the eigenvalues of $J(E_0)$ are the same as above except those associated with C_m and C_b , which are equal to zero. Therefore, in this case, by considering the second order approximations of the right hand sides of Equations (7) and (8), instead of just the first order approximations, and using similar arguments as above, proves that the set B is a local attractor set of A . \square

Theorem A2. *The equilibrium $E_1 = (0, 0, 0, 0, 0, 0, 0, K_{lb}(1 - d_b/k_{pb}), 0, p_{bs}/q_{bd})$ is locally stable if and only if $d_m \geq k_{pm}$ and $k_{pb} > d_b$.*

Proof of Theorem A2. The Jacobian matrix corresponding to the point E_1 is given by the following lower triangular block matrix

$$J(E_1) = \begin{pmatrix} J_1(E_1) & \mathbf{0} & \mathbf{0} \\ * & J_2(E_1) & \mathbf{0} \\ \mathbf{0} & * & J_3(E_1) \end{pmatrix},$$

where $J_1(E_1)$ has the same expression as $J_1(E_0)$, defined in Theorem A1, and

$$J_2(E_1) = \begin{pmatrix} -d_{c2} & k_3 & 0 \\ 0 & -d_m + k_{pm} & 0 \\ 0 & d_m & d_b - k_{pb} \end{pmatrix}, \quad J_3(E_1) = \begin{pmatrix} -q_{cd2}K_{lb}(1 - \frac{d_b}{k_{pb}}) & 0 \\ 0 & -q_{bd}K_{lb}(1 - \frac{d_b}{k_{pb}}) \end{pmatrix}.$$

Since $d_m - k_{pm} \geq 0$ and $k_{pb} > d_b$, and all of the eigenvalues of $J_1(E_0)$ are non-positive values, then the eigenvalues of $J(E_1)$ are negative, except the eigenvalues associated with D and C_m when $k_{pm} = d_m$, which are equal to zero. Therefore, E_1 is a locally stable node, since $D' \leq 0$ for all the variables of the system (1)–(10) and $C'_m \leq 0$ when $k_{pm} = d_m$. \square

Theorem A3. *The equilibrium $E_2 = (0, 0, 0, 0, 0, c_2^*, C_m^*, C_b^*, m_c^*, p_{bs}/q_{bd})$ is locally stable if and only if $k_{pm} > d_m$, where $C_m^* = K_{lm}(1 - d_m/k_{pm})$, $C_b^* = K_{lb}(k_{pb} - d_b + \sqrt{(k_{pb} - d_b)^2 + 4k_{pb}d_m C_m^*/K_{lb}})/2k_{pb}$, $c_2^* = a_{22}(-1 + \sqrt{1 + 4k_3 C_m^*/a_{22}d_{c2}})/2$, and $m_c^* = p_{cs}C_m^*/(q_{cd1}C_m^* + q_{cd2}C_b^*)$.*

Proof of Theorem A3. The Jacobian matrix corresponding to the point E_2 is given by the following lower triangular block matrix

$$J(E_2) = \begin{pmatrix} J_1(E_2) & \mathbf{0} & \mathbf{0} \\ * & J_2(E_2) & \mathbf{0} \\ \mathbf{0} & * & J_3(E_2) \end{pmatrix},$$

where

$$J_1(E_2) = \begin{pmatrix} 0 & 0 & \mathbf{0} & 0 \\ k_{max} & -d_0 - G_2^* & \mathbf{0} & 0 \\ \mathbf{0} & * & J_{11} & \mathbf{0} \\ k_0 H_1^* & 0 & * & -d_{c1} \end{pmatrix}, \quad J_3(E_2) = \begin{pmatrix} -q_{cd1}C_m^* - q_{cd2}C_b^* & 0 \\ 0 & -q_{bd}C_b^* \end{pmatrix},$$

$$J_2(E_2) = \begin{pmatrix} -d_{c2} \left(1 + \frac{c_2^*}{a_{22} + c_2^*}\right) & k_3 H_2^* & 0 \\ 0 & d_m - k_{mb} & 0 \\ 0 & d_m & -\sqrt{(d_b - k_{pb})^2 + 4 \frac{k_{pb}d_m C_m^*}{K_{lb}}} \end{pmatrix},$$

$G_2^* = \frac{c_2^* k_{02}}{a_{02} + c_2^*}$, $H_1^* = \frac{a_{12}}{a_{12} + c_2^*}$, $H_2^* = \frac{a_{22}}{a_{22} + c_2^*}$ and J_{11} is defined as in Theorem A1. Since all of the eigenvalues of J_{11} are negative (Theorem A1) and $k_{pm} > d_m$, and all equilibrium variables and parameter values are positive, then all the eigenvalues of $J_1(E_2)$, $J_2(E_2)$, $J_3(E_2)$ are negative, except for the eigenvalue associated to D which is equal to zero. Therefore, since $D' \leq 0$ for all the variable system, then E_2 is locally stable. \square

References

- Schmidt-Bleek, K.; Kwee, B.J.; Mooney, D.J.; Duda, G.N. Boon and bane of inflammation in bone tissue regeneration and its link with angiogenesis. *Tissue Eng. Part B Rev.* **2015**, *21*, 354–364. [[CrossRef](#)] [[PubMed](#)]
- Kovach, T.K.; Dighe, A.S.; Lobo, P.I.; Cui, Q. Interactions between MSCs and immune cells: Implications for bone healing. *J. Immunol. Res.* **2015**, *2015*, 752510. [[CrossRef](#)] [[PubMed](#)]
- Loi, F.; Córdova, L.A.; Pajarinen, J.; Lin, T.; Yao, Z.; Goodman, S.B. Inflammation, fracture and bone repair. *Bone* **2016**, *86*, 119–130. [[CrossRef](#)] [[PubMed](#)]
- Pisani, P.; Renna, M.D.; Conversano, F.; Casciaro, E.; Di Paola, M.; Quarta, E.; Muratore, M.; Casciaro, S. Major osteoporotic fragility fractures: Risk factor updates and societal impact. *World J. Orthop.* **2016**, *7*, 171. [[CrossRef](#)] [[PubMed](#)]
- Teng, G.G. Mortality and osteoporotic fractures: Is the link causal, and is it modifiable? *Clin. Exp. Rheumatol.* **2008**, *26*, 125.
- Carlier, A.; Geris, L.; Lammens, J.; Van Oosterwyck, H. Bringing computational models of bone regeneration to the clinic. *Wiley Interdisciplin. Rev. Syst. Biol. Med.* **2015**, *7*, 183–194. [[CrossRef](#)] [[PubMed](#)]
- Huber-Lang, M.; Kovtun, A.; Ignatius, A. The role of complement in trauma and fracture healing. *Semin. Immunol.* **2013**, *25*, 73–78. [[CrossRef](#)]
- Foundation, I.O. *Osteoporosis Facts and Statistics*; Data and Publication, International Osteoporosis Foundation: Nyon, Switzerland, 2017.
- Zhou, Z.; Redaelli, A.; Johnell, O.; Willke, R.J.; Massimini, G. A retrospective analysis of health care costs for bone fractures in women with early-stage breast carcinoma. *Cancer* **2004**, *100*, 507–517. [[CrossRef](#)]
- Pajarinen, J.; Lin, T.; Gibon, E.; Kohno, Y.; Maruyama, M.; Nathan, K.; Lu, L.; Yao, Z.; Goodman, S.B. Mesenchymal stem cell-macrophage crosstalk and bone healing. *Biomaterials* **2018**. [[CrossRef](#)]
- Kojouharov, H.V.; Trejo, I.; Chen-Charpentier, B.M. Modeling the effects of inflammation in bone fracture healing. *AIP Conf. Proc.* **2017**, *1895*, 020005.
- Schlundt, C.; El Khassawna, T.; Serra, A.; Dienelt, A.; Wendler, S.; Schell, H.; van Rooijen, N.; Radbruch, A.; Lucius, R.; Hartmann, S.; et al. Macrophages in bone fracture healing: Their essential role in endochondral ossification. *Bone* **2018**, *106*, 78–89. [[CrossRef](#)] [[PubMed](#)]
- Zhang, R.; Liang, Y.; Wei, S. M2 macrophages are closely associated with accelerated clavicle fracture healing in patients with traumatic brain injury: A retrospective cohort study. *J. Orthop. Surg. Res.* **2018**, *13*, 213. [[CrossRef](#)]
- Marsell, R.; Einhorn, T.A. The biology of fracture healing. *Injury* **2011**, *42*, 551–555. [[CrossRef](#)] [[PubMed](#)]
- Chung, E.; Son, Y. Crosstalk between mesenchymal stem cells and macrophages in tissue repair. *Tissue Eng. Regen. Med.* **2014**, *11*, 431–438. [[CrossRef](#)]
- Schlundt, C.; Schell, H.; Goodman, S.B.; Vunjak-Novakovic, G.; Duda, G.N.; Schmidt-Bleek, K. Immune modulation as a therapeutic strategy in bone regeneration. *J. Exp. Orthop.* **2015**, *2*, 1. [[CrossRef](#)] [[PubMed](#)]
- Chan, J.K.; Glass, G.E.; Ersek, A.; Freidin, A.; Williams, G.A.; Gowers, K.; Santo, A.I.E.; Jeffery, R.; Otto, W.R.; Poulosom, R.; et al. Low-dose TNF augments fracture healing in normal and osteoporotic bone by up-regulating the innate immune response. *EMBO Mol. Med.* **2015**, *7*, 547–561. [[CrossRef](#)] [[PubMed](#)]
- Mantovani, A.; Sozzani, S.; Locati, M.; Allavena, P.; Sica, A. Macrophage polarization: Tumor-associated macrophages as a paradigm for polarized M2 mononuclear phagocytes. *Trends Immunol.* **2002**, *23*, 549–555. [[CrossRef](#)]
- Border, W.A.; Noble, N.A. Transforming growth factor β in tissue fibrosis. *N. Engl. J. Med.* **1994**, *331*, 1286–1292.
- Cavaillon, J.M. Pro-versus anti-inflammatory cytokines: Myth or reality. *Cell. Mol. Biol.* **2001**, *47*, 695–702.
- Osta, B.; Benedetti, G.; Miossec, P. Classical and paradoxical effects of TNF- α on bone homeostasis. *Front. Immunol.* **2014**, *5*, 48. [[CrossRef](#)]

22. Arango Duque, G.; Descoteaux, A. Macrophage cytokines: Involvement in immunity and infectious diseases. *Front. Immunol.* **2014**, *5*, 491. [[CrossRef](#)] [[PubMed](#)]
23. Mountziaris, P.M.; Mikos, A.G. Modulation of the inflammatory response for enhanced bone tissue regeneration. *Tissue Eng. Part B Rev.* **2008**, *14*, 179–186. [[CrossRef](#)] [[PubMed](#)]
24. Gibon, E.; Lu, L.Y.; Nathan, K.; Goodman, S.B. Inflammation, ageing, and bone regeneration. *J. Orthop. Transl.* **2017**, *10*, 28–35. [[CrossRef](#)] [[PubMed](#)]
25. Gibon, E.; Loi, F.; Córdova, L.A.; Pajarinen, J.; Lin, T.; Lu, L.; Nabeshima, A.; Yao, Z.; Goodman, S.B. Aging affects bone marrow macrophage polarization: Relevance to bone healing. *Regen. Eng. Transl. Med.* **2016**, *2*, 98–104. [[CrossRef](#)] [[PubMed](#)]
26. Serhan, C.N.; Savill, J. Resolution of inflammation: The beginning programs the end. *Nat. Immunol.* **2005**, *6*, 1191–1197. [[CrossRef](#)] [[PubMed](#)]
27. Newman, S.L.; Henson, J.E.; Henson, P.M. Phagocytosis of senescent neutrophils by human monocyte-derived macrophages and rabbit inflammatory macrophages. *J. Exp. Med.* **1982**, *156*, 430–442. [[CrossRef](#)]
28. Italiani, P.; Boraschi, D. From monocytes to M1/M2 macrophages: Phenotypical vs. functional differentiation. *Front. Immunol.* **2014**, *5*, 514. [[CrossRef](#)]
29. Wang, Y.; Yang, T.; Ma, Y.; Halade, G.V.; Zhang, J.; Lindsey, M.L.; Jin, Y.F. Mathematical modeling and stability analysis of macrophage activation in left ventricular remodeling post-myocardial infarction. *BMC Genom.* **2012**, *13*, S21. [[CrossRef](#)]
30. Bailon-Plaza, A.; Van Der Meulen, M.C. A mathematical framework to study the effects of growth factor influences on fracture healing. *J. Theor. Biol.* **2001**, *212*, 191–209. [[CrossRef](#)]
31. Echeverri, L.; Herrero, M.; Lopez, J.; Oleaga, G. Early stages of bone fracture healing: Formation of a fibrin–collagen scaffold in the fracture hematoma. *Bull. Math. Biol.* **2015**, *77*, 156–183. [[CrossRef](#)]
32. Doblaré, M.; Garcia, J.; Gómez, M. Modelling bone tissue fracture and healing: A review. *Eng. Fract. Mech.* **2004**, *71*, 1809–1840. [[CrossRef](#)]
33. Ghiasi, M.S.; Chen, J.; Vaziri, A.; Rodriguez, E.K.; Nazarian, A. Bone fracture healing in mechanobiological modeling: A review of principles and methods. *Bone Rep.* **2017**, *6*, 87–100. [[CrossRef](#)] [[PubMed](#)]
34. Einhorn, T.A. The science of fracture healing. *J. Orthop. Trauma* **2005**, *19*, S4–S6. [[CrossRef](#)] [[PubMed](#)]
35. Einhorn, T.A.; Gerstenfeld, L.C. Fracture healing: Mechanisms and interventions. *Nat. Rev. Rheumatol.* **2015**, *11*, 45. [[CrossRef](#)] [[PubMed](#)]
36. Gómez-Barrena, E.; Rosset, P.; Lozano, D.; Stanovici, J.; Ernthaller, C.; Gerbhard, F. Bone fracture healing: Cell therapy in delayed unions and nonunions. *Bone* **2015**, *70*, 93–101. [[CrossRef](#)] [[PubMed](#)]
37. Carlier, A.; Geris, L.; van Gastel, N.; Carmeliet, G.; Van Oosterwyck, H. Oxygen as a critical determinant of bone fracture healing—A multiscale model. *J. Theor. Biol.* **2015**, *365*, 247–264. [[CrossRef](#)] [[PubMed](#)]
38. Nagaraja, S.; Wallqvist, A.; Reifman, J.; Mitrophanov, A.Y. Computational approach to characterize causative factors and molecular indicators of chronic wound inflammation. *J. Immunol.* **2014**, *192*, 1824–1834. [[CrossRef](#)] [[PubMed](#)]
39. Yu, T. Design and Validation of A Mathematical Model to Describe Macrophage Dynamics in Wound Healing. Ph.D. Thesis, Drexel University, Philadelphia, PA, USA, 2014.
40. Otto, S.P.; Day, T. *A Biologist's Guide to Mathematical Modeling in Ecology and Evolution*; Princeton University Press: Princeton, NJ, USA, 2011.
41. Marée, A.F.; Komba, M.; Dyck, C.; Labkecki, M.; Finegood, D.T.; Edelstein-Keshet, L. Quantifying macrophage defects in type 1 diabetes. *J. Theor. Biol.* **2005**, *233*, 533–551. [[CrossRef](#)]
42. Sherratt, J.A.; Murray, J. Models of epidermal wound healing. *Proc. R. Soc. Lond. B* **1990**, *241*, 29–36.
43. Isaksson, H. Recent advances in mechanobiological modeling of bone regeneration. *Mech. Res. Commun.* **2012**, *42*, 22–31. [[CrossRef](#)]
44. Schell, H.; Duda, G.; Peters, A.; Tsitsilonis, S.; Johnson, K.; Schmidt-Bleek, K. The haematoma and its role in bone healing. *J. Exp. Orthop.* **2017**, *4*, 5. [[CrossRef](#)] [[PubMed](#)]
45. Van Furth, R.; Diesselhoff-den Dulk, M.M.; Mattie, H. Quantitative study on the production and kinetics of mononuclear phagocytes during an acute inflammatory reaction. *J. Exp. Med.* **1973**, *138*, 1314–1330. [[CrossRef](#)] [[PubMed](#)]

46. Bastidas-Coral, A.P.; Bakker, A.D.; Zandieh-Doulabi, B.; Kleverlaan, C.J.; Bravenboer, N.; Forouzanfar, T.; Klein-Nulend, J. Cytokines TNF- α , IL-6, IL-17F, and IL-4 differentially affect osteogenic differentiation of human adipose stem cells. *Stem Cells Int.* **2016**, *2016*, 1318256. [[CrossRef](#)] [[PubMed](#)]
47. Gilbert, L.; He, X.; Farmer, P.; Boden, S.; Kozlowski, M.; Rubin, J.; Nanes, M.S. Inhibition of Osteoblast Differentiation by Tumor Necrosis Factor- α 1. *Endocrinology* **2000**, *141*, 3956–3964. [[CrossRef](#)] [[PubMed](#)]
48. Lacey, D.; Simmons, P.; Graves, S.; Hamilton, J. Proinflammatory cytokines inhibit osteogenic differentiation from stem cells: Implications for bone repair during inflammation. *Osteoarthritis Cartilage* **2009**, *17*, 735–742. [[CrossRef](#)] [[PubMed](#)]
49. Lu, Y.; Lekszycki, T. Modeling of an initial stage of bone fracture healing. *Contin. Mech. Thermodyn.* **2015**, *27*, 851. [[CrossRef](#)]
50. Hoegel, F.; Abdulazim, A.; Augat, P.; Buehren, V. Quantification of reaming debris at the fracture gap of diaphyseal A2 and A3 Fractures After reamed intramedullary nailing of the sheep tibia. *Eur. J. Trauma Emerg. Surg.* **2008**, *34*, 587–591. [[CrossRef](#)]
51. Gaston, M.; Simpson, A. Inhibition of fracture healing. *Bone Joint J.* **2007**, *89*, 1553–1560. [[CrossRef](#)]
52. Roberts, T.T.; Rosenbaum, A.J. Bone grafts, bone substitutes and orthobiologics: The bridge between basic science and clinical advancements in fracture healing. *Organogenesis* **2012**, *8*, 114–124. [[CrossRef](#)]
53. Wu, M.; Chen, G.; Li, Y.P. TGF- β and BMP signaling in osteoblast, skeletal development, and bone formation, homeostasis and disease. *Bone Res.* **2016**, *4*, 16009. [[CrossRef](#)]
54. Recknagel, S.; Bindl, R.; Brochhausen, C.; Göckelmann, M.; Wehner, T.; Schoengraf, P.; Huber-Lang, M.; Claes, L.; Ignatius, A. Systemic inflammation induced by a thoracic trauma alters the cellular composition of the early fracture callus. *J. Trauma Acute Care Surg.* **2013**, *74*, 531–537. [[CrossRef](#)] [[PubMed](#)]
55. Stuart, A.; Humphries, A.R. *Dynamical Systems and Numerical Analysis*; Cambridge University Press: Cambridge, UK, 1998.
56. Strang, G. *Introduction to Linear Algebra*; Wellesley-Cambridge Press: Wellesley, MA, USA, 1993.



© 2019 by the authors. Licensee MDPI, Basel, Switzerland. This article is an open access article distributed under the terms and conditions of the Creative Commons Attribution (CC BY) license (<http://creativecommons.org/licenses/by/4.0/>).